Analytical Channel Model and Link Design Optimization for Ground-to-HAP Free-Space Optical Communications

Analytical Channel Model and Link Design Optimization for Ground-to-HAP Free-Space Optical Communications

Hossein Safi, Akbar Dargahi, Julian Cheng, *Senior Member, IEEE*, and Majid Safari, *Member, IEEE*

***Abstract*—Integrating high altitude platforms (HAPs) and free space optical (FSO) communications is a promising solution to establish high data rate aerial links for the next generation wireless networks. However, practical limitations such as pointing errors and angle-of-arrival (AOA) fluctuations of the optical beam due to the orientation deviations of hovering HAPs make it challenging to implement HAP-based FSO links. For a ground-to-HAP FSO link, tractable, closed-form statistical channel models are derived in this paper to simplify optimal design of such systems. The proposed models include the combined effects of atmospheric turbulence regimes (i.e., log-normal and gamma-gamma), pointing error induced geometrical loss, pointing jitter variance caused by beam wander, detector aperture size, beam-width, and AOA fluctuations of the received optical beam. The analytical expressions are corroborated by performing Monte-Carlo simulations. Furthermore, closed-form expressions for the outage probability of the considered link under different turbulence regimes are derived. Detailed analysis is carried out to optimize the transmitted laser beam and the field-of-view of the receiver for minimizing outage probability under different channel conditions. The obtained analytical results can be applied to finding the optimal parameter values and designing ground-to-HAP FSO links without resorting to time-consuming simulations.**

***Index Terms*—Angle-of-arrival fluctuations, atmospheric turbulence, channel modeling, free-space optics, high altitude platforms.**

I. Introduction

Recently, high altitude platforms (HAPs) have received considerable attention as a promising candidate to extend the coverage of terrestrial networks by providing easy-to-deploy and cost-effective links [1]. HAP systems are preferable for providing broadband communications and wide-scale wireless coverage for large geographic areas [2]. In particular, HAPs can be used either as aerial relays to improve ubiquitous connectivity of terrestrial wireless systems, or as flying base stations (BSs) to provide reliable downlink and uplink communications for ground users [3]. Free space optical (FSO)-based front-haul/back-haul links are proposed as a promising approach for the next generation of wireless networks to confront the challenge of scarce radio spectrum resources and to obtain high data rate transmission on the order of Gbps [4], [5]. To support FSO communications, as shown in Fig. 1, HAPs can be considered as superior candidates. In particular, unique capabilities of HAPs, e.g., maneuverability and adaptive altitude adjustment enable them to effectively establish line-of-sight (LoS) communication links that are necessary for successful data transmission in an FSO link. As examples, Google's Project Loon and Facebook's Internet-delivery drone are the two recent projects that combines FSO communications with HAPs [6], [7][1].

However, for successful implementation, FSO links suffer from practical limitations. First, FSO communication is sensitive to beam alignment from transmitter to receiver. Therefore, it is essential to perform accurate beam pointing at the transmitter side, and beam acquisition and tracking at the receiver side. With an array of photo-detectors located at the focal plane of the receiver, a spatial beam tracking method was proposed for a ground-to-drone FSO link to tackle the effect of hovering fluctuations of the receiver [10]. Moreover, there exist accurate beam tracking methods based on mechanical or piezoelectric equipment, e.g., gimbals and retro reflectors, which are readily applicable for mobile FSO communications [11], [12]. A recent comprehensive literature review [13] discussed existing beam acquisition and tracking mechanisms suitable for mobile FSO communications and categorized these mechanisms according to their working principles, use cases, their advantages and disadvantages.

Second, beam wander and scintillation due to inhomogeneity in temperature and pressure of the air can severely affect the link performance [14]. To tackle the effect of atmospheric turbulence, different fading mitigation techniques such as novel sequence data detection algorithms [15], [16], temporal and spatial diversity [17]–[19], aperture averaging, adaptive optics, and adaptive channel coding [20] have been proposed in the context of FSO. For instance, the authors in [15] propose a Viterbi-type trellis-search sequence receiver based on the generalized likelihood ratio test principle that jointly detects the data sequence and estimates the unknown channel

H. Safi, and A. Dargahi are with the Department of Electrical Engineering, Shahid Beheshti University G. C., 1983963113, Tehran, Iran (e-mails: {h_safi, a-dargahi}@sbu.ac.ir). J. Cheng is with the School of Engineering, the University of British Columbia, V1V 1V7, Kelowna, BC Canada (e-mail: julian.cheng@ubc.ca). M. Safari is with the School of Engineering, the University of Edinburgh, EH8 9YL, Edinburgh, UK (e-mail: msafari@exseed.ed.ac.uk)

[1]It is worth noting that, as proposed and implemented in [8], [9], there exist spaceborne optical communication links (i.e., high data-rate bi-directional optical communications between Earth and geostationary Earth orbit (GEO), and low Earth orbit (LEO)) which employ adaptive optics (AO) to facilitate coupling the received optical signal into a single-mode fiber. In this regard, the AO system should be capable of coupling more than half the received signal into the single mode fiber. Due its technical complexity and implementation cost as well as it narrow scopes (which are mainly limited to deep space communications), in this paper, we do not consider these types of FSO communication systems which employ the AO subsystem in their links.

Fig. 1. A typical illustration of a HAP-based FSO communication link. HAPs are usually placed in the stratosphere layer where the thin air is relatively calm and the wind speed is low, and thus, the link length is commonly larger than 17 km [1].

gain. The work in [17] considers a multiple-input multiple-output with optical space shift keying signaling scheme and employs receiver diversity to efficiently combat the turbulence effects. Moreover, the authors in [18] utilize a distributed photon-counting receiver array as a cost-effective and adaptable alternative approach to traditional large, single-aperture receive elements. The work in [19] uses multiple transmitter to compensate scintillation fades. Meanwhile, the authors in [20] present adaptive coding and power transmission schemes to tackle the effect of atmospheric turbulence in a practical FSO communication system. The turbulence effect can also be reduced by adaptive optics [21]–[23]. By this technique, the distortion induced in the wave-front by the atmospheric turbulence is reduced through the use of wavefront sensors and deformable mirrors [24], [25]. However, the application of this technique is very limited and it does not seem to be of interest in commercial FSO systems due to its high and unjustified implementation complexity and cost [24]. In addition, its effectiveness to compensate the effects of atmospheric turbulence is practically limited to relatively short-range links [25], [26].

Third, mounting the optical receiver on a HAP station can cause the angle-of-arrival (AOA) fluctuations due to orientation deviations of the receiver, which in turn induce signal-to-noise ratio (SNR) fluctuations and significantly degrade the reliability of the system [27]. Indeed, such degradation factors are distance-dependent and their effects are significant on long-range FSO links, which is usually the case for HAP-based FSO systems. Therefore, the impairments caused by these factors should be taken into account when evaluating the performance of such communication systems.

To assess the benefits of a ground-to-HAP FSO link, the communication channel should be distinctively characterized in terms of the receiver random vibrations due to hovering fluctuations and optical beam propagation characteristics in the atmosphere. Although, there has been a surge of recent works on drone based FSO communications [4], [5], [28]–[32], these prior works all assumed stable drones and did not address the presence of AOA fluctuations and position vibrations. Recently, studies have been reported on the effects of random fluctuations in the aperture position and orientation as well as atmospheric turbulence loss and attenuation. For examples, a multi rotor drone-based FSO link was modeled to take into consideration of the effects due to position and AOA fluctuations [33]. However, the proposed model is quite complex and not so tractable for further research investigations. More recently, a simpler and tractable channel model for the considered system model in [33] are proposed in [34] over log-normal atmospheric turbulence environment. However, the authors in [33], [34] ignored the effects of the side-lobes of optical Airy pattern at the receiver which result in an outage probability floor. Meanwhile, based on the assumption of non-orthogonal incident beam to the photo detector (PD) plane, a statistical model was proposed for the geometrical and misalignment losses of the FSO channel for unmanned aerial vehicles (UAVs)-based networks [35], where the background noise was assumed as the dominant noise source at the PD. However, in this noise regime, the receiver field-of-view (FOV) was not optimized to mitigate the effects of background noise and orientation deviations of the UAV. In the aforementioned works, it is commonly assumed that the transceiver has the same altitude (i.e., not a slant path). In addition, the effect of beam wander is typically neglected due to short link length (low-altitude assumptions), and also the pointing error geometrical loss model is developed based on Gaussian beam profile. However, this assumptions may not hold for a HAP-based FSO system. Because the transceivers in such systems do not have the same altitude, and also the link distance is long. As a result, plane wave and spherical wave models are more accurate optical wave models than the Gaussian beam profile [14], [36] for presenting the characteristic of beam profile at the receiver.

In this paper, we drive analytical channel models for ground-to-HAP FSO links by taking into account the effects of atmospheric attenuation and turbulence (both log-normal (LN) and gamma-gamma (GG) turbulence models), pointing error induced geometrical loss, and the effects of hovering fluctuations of the HAP, i.e., position vibrations of the optical receiver as well as the AOA fluctuations of the received optical beam. We first consider optical beam profile at the receiver for a long-range FSO link, and propose a new statistical model for pointing error induced geometrical loss. This model incorporates the position vibrations of the receiver, pointing jitter variance caused by beam wander, detector aperture size and received optical beam-width. Using the developed pointing error model, we drive closed-form expressions for the channel model of the

considered link under different turbulence regimes, i.e., weak and moderate to strong atmospheric turbulence conditions. For FSO systems, the coherence time of the communication channel is on the order of 1-100 msec which is significantly greater than the typical nanosecond bit duration (or equally Gbps transmission rate) [37]. Therefore, for such slow fading channels, outage probability, which is the probability of the event when the instantaneous SNR falls bellow a certain threshold, is the most relevant metric to evaluate system performance [24]. Accordingly, we derive closed-form expressions for the outage probability of the considered link for both LN and GG atmospheric turbulence models. Moreover, we provide a detailed analysis for optimizing the transmitted laser beam by tuning divergence angle of the transmitter and the FOV of the receiver to achieve minimum outage probability under different channel conditions. In particular, we show that optimizing the beam-width of the transmitter calls for balancing a tradeoff between the amounts of pointing error and effective transmitter gain. Furthermore, when optimizing the receiver FOV, a compromise is required between the amount of undesired background power and mitigation of beam position deviation, which is due to hovering fluctuations. Simulation results are provided to validate the derived analytical expressions of channel model and outage probability. Thus, from the developed analytical expressions for channel modeling and outage probability, performance evaluation of the ground-to-HAP FSO links can be carried out without resorting to time-consuming simulations.

The rest of the paper is organized as follows. Section II presents the system model. In Section III, we introduce the statistical model for pointing error induced geometrical loss and derive channel distribution functions and outage probability of the considered link. In Section IV, numerical results are provided to demonstrate the need for optimizing receiver divergence angle and transmitter FOV under different channel conditions. Finally, we conclude the paper in Section V.

II. System Model

The schematic of the considered optical uplink is shown in Fig. 2 where a ground station transmits optical signals towards an aerial platform. We assume that the aerial-based receiver is hovering at a distance Z from the ground transmitter. Also, the mean position of the receiver is $H_R = (0, 0, 0)$, and its location is known to the transmitter. Regarding H_R, the instantaneous position of the HAP is indicated by $H_d = (d_x, d_y, d_z)$, where the independent random variables (RVs) d_x, d_y, and d_z denote random deviations along the axes of coordinates. Since the link length Z is much larger than the variance of RV d_z, compared to the RVs d_x and d_y, one can reasonably assume to neglect the amount of vibration along the z-axis. In practice, due to the effects of hovering, the aperture position and orientation can deviate away from their means, causing fluctuations in the AOA of the received optical beam. Accordingly, the independent RVs of orientation deviations of the HAP are denoted by θ_{Rx} and θ_{Ry} in $x-z$ plane and $y-z$ plane, respectively. We also assume that the instantaneous

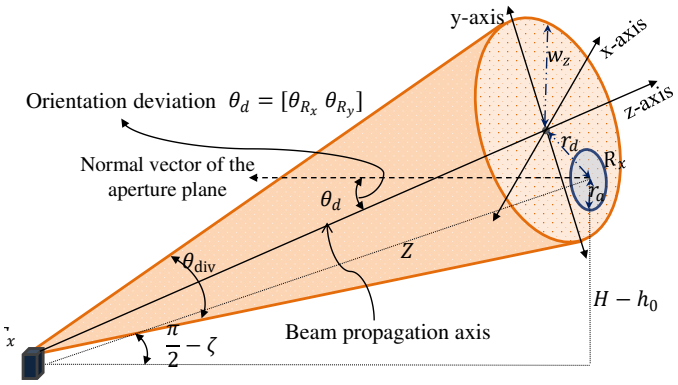

Fig. 2. The schematic of the considered optical uplink. Link parameters are defined as follows. Z is the link length, H is the HAP altitude, h_0 is the transmitter altitude, θ_{div} is the divergence angle of the optical transmitter, ζ is the HAP zenith angle, r_d denotes the separation distance between the center of optical beam footprint and the center of the receiver aperture, r_a is the aperture radius, and w_Z is the radius of the received optical beam at distance Z. Also, the orientation deviations of the HAP are indicated by θ_{Rx} and θ_{Ry} in $x-z$ plane and $y-z$ plane, respectively.

position and the orientation deviations of the HAP node are Gaussian distributed [33], i.e., d_x, $d_y \sim \mathcal{N}(0, \sigma_d^2)$, and θ_{Rx}, $\theta_{Ry} \sim \mathcal{N}(0, \sigma_0^2)$. Moreover, at the receiver aperture, the random displacements of the centroid of the propagated beam due to beam wander effects along the x and y coordinates, namely b_x and b_y, are approximately Gaussian distributed with mean zero and variance [32]

$$\sigma_b^2 = 2.07 \int_{h_0}^{H} C_n^2(l) (Z-l)^2 w_h^{-\frac{1}{3}} dl \tag{1}$$

where H, h_0, and w_l are respectively the HAP altitude, the transmitter altitude, and the beam-width at distance l. The propagation distance Z is given by $(H - h_0)\sec(\zeta)$, where ζ is the HAP zenith angle[1]. Moreover, In (1), $C_n^2(l)$ is the refractive-index structure parameter that describes the varying strength of optical turbulence as a function of altitudes l, and it can be obtained as [14, p.481]

$$\begin{aligned} C_n^2(l) = \ & 0.00594 (V_w/27)^2 \left(10^{-5} l\right)^{10} e^{-l/1000} \\ & + 2.7 \times 10^{-16} e^{-l/1500} + S_t e^{-l/100} \end{aligned} \tag{2}$$

where V_w is the root-mean-square (rms) wind speed in meter per second (m/s), and S_t is the nominal value of $C_n^2(0)$ at the ground in $\text{m}^{-2/3}$.

The incoming optical beam is focused onto the PD through the lens. Due to the scattered sunlight, the PD inevitably collects undesired background light. Assuming intensity modulation at the transmitter and direct detection at the receiver, the PD converts the optical signal to an electrical current. For the ith symbol interval, the output photo-current can be obtained as [38]

$$r[i] = \eta\, h\, s[i] + n[i] \tag{3}$$

where η, h, $s[i]$, and $n[i]$ are, respectively, the PD responsibility, the channel coefficient, the transmitted symbol with

[1]Zenith angle is the angle between two straight lines from the ground transmitter to the HAP and the zenith point.

average optical power P_t, and the signal-independent zero-mean Gaussian noise with variance σ_n^2. Under the assumption of background noise as the dominant noise source at the receiver, the noise variance σ_n^2 can be expressed as [14]

$$\sigma_n^2 = 2eB_e\eta P_b \tag{4}$$

where e is the electron charge, B_e denotes the bandwidth of the PD, and P_b is the power of background light. Also, we have [14]

$$P_b = N_b B_o \Omega_{\text{FOV}} A_r \tag{5}$$

where N_b denotes the spectral radiance of the background radiations at wavelength λ[2], B_o stands for the bandwidth of the optical filter at the receiver, and A_r denotes the aperture area. It is worth mentioning that, the spectral radiance of the sky, $N_b(\lambda)$, is measured for a rectangular portion of the horizon sky under various weather conditions and at different solar positions [39]–[41]. Accordingly, it is a function of wavelength, zenith angle, and azimuth angle between the telescope, the target and the Sun, and is commonly derived by sequentially measuring a set of directions in the sky (i.e., sky scanning). Moreover, the sky radiance for different parameters has been computed using MODTRAN, a worldwide computer program designed to model atmospheric propagation of electromagnetic radiation, and the results are provided in [42]. For instance, from the result of [42] and for $\lambda = 1500$ nm, solar zenith angle of 45°, and azimuthal angle of 0°, the spectral radiance is equal to 10^{-3} W/cm^2-m-srad.

Also, Ω_{FOV} in (5) is the receiver FOV, i.e., the solid angle through which the receiver can capture the transmitted laser beam, and it is obtained in the spherical coordinate system as

$$\Omega_{\text{FOV}} = 2\pi\big(1 - \cos(\theta_{\text{FOV}}/2)\big) \tag{6}$$

where $\theta_{\text{FOV}} = 2\arctan(\frac{r_p}{f_c})$, and where r_p and f_c are, respectively, the radius of the circular PD and focal length of the aperture. Furthermore, the instantaneous electrical signal-to-noise ratio (SNR) is obtained as [14]

$$\gamma = \frac{\eta^2 P_t^2 h^2}{\sigma_n^2}. \tag{7}$$

Since in FSO systems the coherence time of all different channel variables are long relative to the bit duration (i.e., slow fading channel), when no fading-mitigation technique such as aperture averaging, diversity, or adaptive optics is employed, outage probability becomes more meaningful for evaluating the systems performance. [43]. Accordingly, the outage probability is defined as the probability that the instantaneous SNR is less than a threshold γ_{th}, and it can be written as

$$\mathbb{P}_{\text{out}} = \int_0^{\gamma_{\text{th}}} f_\gamma(\gamma)d\gamma \tag{8}$$

where $f_\gamma(\gamma)$ is the probability density function (PDF) of γ. Since γ is a monotonically increasing function of h, the outage probability can be also obtained as

$$\mathbb{P}_{\text{out}} = \int_0^{h_{\text{th}}} f_h(h)dh \tag{9}$$

where $h_{\text{th}} = \frac{\sqrt{\gamma_{\text{th}}\sigma_n^2}}{\eta P_t}$, and $f_h(h)$ is the PDF of h.

III. Channel Modeling

Four channel parameters are incorporated into h, i.e.,

$$h = \underbrace{h_{al}h_{at}h_{pl}}_{h_{ag}}h_{af} \tag{10}$$

where h_{al}, h_{at}, h_{pl}, and h_{af} stand for the attenuation loss, the atmospheric turbulence, the effective pointing error induced geometrical loss, and the link interruption due to the AOA fluctuations at the receiver, respectively. In the sequel, the link interruption parameter h_{af} takes two discrete values "1" or "0" to indicate the presence or absence of received beam in the receiver FOV.

A. Attenuation loss and Atmospheric Turbulence

For an optical link with length Z, the attenuation loss is represented by the Beers-Lambert law as $h_{al} = \exp(-Z\xi)$, where ξ is the attenuation coefficient related to the visibility [44]. To model the atmospheric turbulence induced fading, we consider both LN and GG atmospheric turbulence models. Accordingly, the LN model is appropriate for weak turbulence conditions whereas the GG model is a suitable statistical model for moderate to strong atmospheric turbulence conditions [14]. The PDF of h_{at} based on the LN model is obtained as

$$f_{\text{LN}}(h_{at}) = \frac{1}{2h_{at}\sqrt{2\pi\sigma_{Bu}^2}}\exp\left(-\frac{(\ln h_{at} + 2\sigma_{Bu}^2)^2}{8\sigma_{Bu}^2}\right) \tag{11}$$

where σ_{Bu}^2 is the Rytov variance. Note that, the transceivers in our setup are not located at the same height (i.e., a slant path), σ_{Bu}^2 is obtained as[3] [14]

$$\begin{aligned}\sigma_{Bu}^2 =& 2.25\left(\frac{2\pi}{\lambda}\right)^{\frac{7}{6}}(H-h_0)^{\frac{5}{6}}\sec(\zeta)^{\frac{11}{6}} \\ &\times\int_{h_0}^{H} C_n^2(l)\left(1-\frac{l-h_0}{H-h_0}\right)^{\frac{5}{6}}\left(\frac{l-h_0}{H-h_0}\right)^{\frac{5}{6}}dl.\end{aligned} \tag{12}$$

Moreover, the PDF of h_{at} according to the GG model is obtained as

$$f_{\text{GG}}(h_{at}) = \frac{2(\alpha\beta)^{\frac{\alpha+\beta}{2}}}{\Gamma(\alpha)\Gamma(\beta)}h_{at}^{\frac{\alpha+\beta}{2}-1}K_{\alpha-\beta}(2\sqrt{\alpha\beta h_{at}}) \tag{13}$$

[2]We note that, for the considered HAP-based FSO link, the choice of wavelength strongly depends on atmospheric effects, attenuation and background noise power, the availability of transmitter and receiver components, eye safety regulations, and cost. Indeed, choosing the operating wavelength requires balancing a tradeoff between the receiver sensitivity and pointing bias due to thermal variations across the Earth's surface. Thus, longer wavelengths are preferred as they make reduction in solar scattering as well as solar background from the Earth surface [25].

[3]The Earth's atmosphere is composed several distinct layers extends to approximately 700 km above the Earth's surface with the heaviest concentration of particles in the first 40 km above the surface (also known as the free atmosphere). In our work we rely on the proposed general profile model, also known as Hufnagle-Valley model, in [14]. The H-V model is well suited for gounod-to-air links and covers the link range of several tens of kilometers (which is the case for the considered HAP-based FSO communications in this work) [45]–[47]. It is worth mentioning that, standard atmospheric spectral models are based on isotropic conditions throughout the free atmosphere. However, there exists evidence that reveals the turbulence above the free atmosphere is nonisotropic. For the communication links longer than 40 km, this will affect the computations of outage probability and the other link parameters.

where $\Gamma(\cdot)$ is the Gamma function and $K_\nu(\cdot)$ is the modified Bessel function of the second kind of order ν. Also, parameters α and β denote the effective numbers of large-scale and small-scale eddies, respectively, and they can be represented as [14]

$$\alpha = \left[\exp\left(0.49\sigma_{Bu}^2 \Big/ \left(1+0.56\sigma_{Bu}^{12/6}\right)^{7/6}\right) - 1\right]^{-1},$$
$$\beta = \left[\exp\left(0.51\sigma_{Bu}^2 \Big/ \left(1+0.69\sigma_{Bu}^{12/6}\right)^{5/6}\right) - 1\right]^{-1}. \quad (14)$$

B. Effective Pointing Error

Considering a Gaussian optical beam at the transmitter, the normalized spatial distribution of the transmitted intensity at distance Z is given by [48]

$$I(\rho; Z) = \frac{2}{\pi\omega_Z^2}\exp\left(-\frac{2||\boldsymbol{\rho}||^2}{\omega_Z^2}\right) \quad (15)$$

where $\boldsymbol{\rho}$ is the radial vector form the center of the optical beam. Also in (15), ω_Z is the beam waist at distance Z and is approximately obtained as [43]

$$\omega_Z \approx w_0\left[1+\epsilon\left(\frac{\lambda Z}{\pi\omega_0^2}\right)^2\right]^{0.5} \quad (16)$$

where ω_0 is the beam waist at $Z=0$, and it is a parameter that can be tuned at the optical transmitter by employing different diameters for the aperture (or equivalently different divergence angles). More precisely, for a transmitter aperture of diameter D, w_0 is equal to $\frac{D}{\sqrt{2}\pi}$ [49]. Also in (16), $\epsilon = \left(1+2\omega_0^2/\rho_0^2\right)$, and $\rho_0 = \int_{h_0}^{H}\left(0.55C_n^2(l)\left(\frac{2\pi}{\lambda}\right)^2 l\right)^{-\frac{3}{5}}dl$ is the coherence length. Let $\boldsymbol{r_d}$ denote the radial beam displacement vector, i.e., the separation distance between the center of optical beam footprint and the center of the receiver aperture due to pointing errors. Therefore, for a circular receiver aperture with radius r_a and the collecting area $A_r = \pi r_a^2$ which is aligned at an angle θ_d with respect to the arriving beam direction, pointing error loss due to geometrical spread can be expressed as

$$h_{pl|\theta_d} = \int_{A_r} I(\boldsymbol{\rho} - \boldsymbol{r_d}; Z)\cos(\theta_d)d\boldsymbol{\rho}. \quad (17)$$

In the considered link, the receiver is located at a distance of Z from the optical transmitter where $\omega_Z \gg r_a$. In this regime, the overall phase of the wave becomes constant and phase difference between different parts of the optical wavefront at the receiver can be ignored. Hence, the optical field at the receiver lens maintains locally the plane wave nature [36], [48]. Thus, when the aperture area is much smaller than the beam waist, we can reasonably assume that the received optical intensity over the aperture area is constant, and we rewrite (17) as

$$h_{pl|\theta_d} \simeq 2\left(\frac{r_a}{\omega_Z^2}\right)^2\exp\left(-\frac{2||\boldsymbol{r_d}||^2}{\omega_Z^2}\right)\cos(\theta_d). \quad (18)$$

As shown in Fig. 3, by taking beam wander effects and instantaneous position of the HAP into consideration, we have

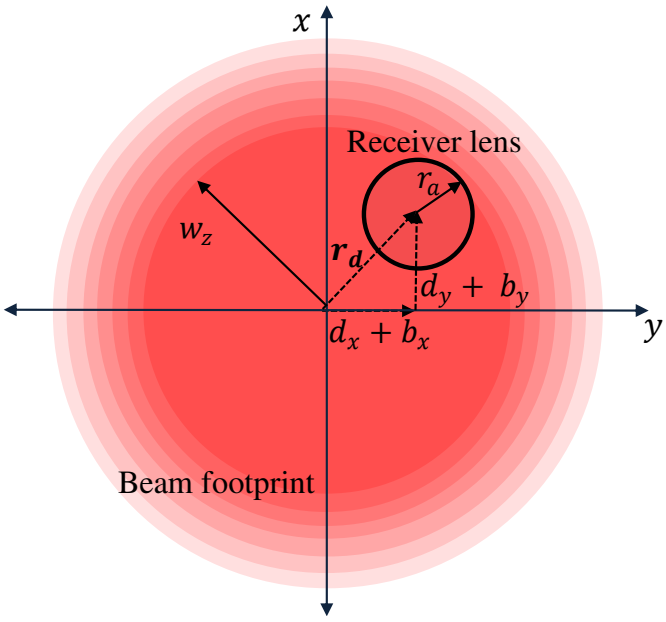

Fig. 3. Received optical beam footprint at the receiver aperture for a long-range ground-to-HAP FSO link. Because of the effects of beam wander as well as hovering fluctuations, the center of the beam is randomly deviated from the center of receiver lens.

$||\boldsymbol{r_d}|| = \sqrt{(d_x+b_x)^2+(d_y+b_y)^2}$. Since d_x and d_y are zero-mean Gaussian RVs with variance σ_d^2, the RV $r_d = ||\boldsymbol{r_d}||$ follows a Rayleigh PDF as

$$f_{r_d}(r_d) = \frac{r_d}{\sigma_r^2}\exp\left(-\frac{r_d^2}{2\sigma_r^2}\right), \quad r_d \geq 0 \quad (19)$$

where $\sigma_r^2 = \sigma_d^2 + \sigma_b^2$. From (18) and (19), and after some manipulations, the PDF of h_{pl} conditioned on θ_d can be derived as

$$f_{h_{pl}|\theta_d}(h_{pl}) = C_1^{-C_3}C_3 {h_{pl}}^{C_3-1}\cos(\theta_d) \quad (20)$$

where $C_1 = 2\left(\frac{r_a}{\omega_Z^2}\right)^2$, $C_2 = \frac{2}{\omega_Z^2}$, and $C_3 = \frac{1}{2C_2\sigma_r^2}$.

Furthermore, the PDF of $h_{ag} = h_{al}h_{at}h_{pl}$ conditioned on θ_d can be obtained as

$$f_{h_{ag}|\theta_d}(h_{ag}) = \int f_{h_{ag}|\theta_d,h_{at}}(h_{ag})f_{h_{at}}(h_{at})dh_{at} \quad (21)$$
$$= \int \frac{1}{h_{al}h_{at}}f_{h_{pl}|\theta_d}\left(\frac{h_{ag}}{h_{al}h_{at}}\right)f_{h_{at}}(h_{at})dh_{at}.$$

Substituting (13), (11) and (20) in (21) and after some manipulations, we obtain the analytical expressions of $f_{h_{ag}|\theta_d}(h_{ag})$ for low values of h and under both LN and GG atmospheric turbulence models in (22), and (23), respectively, where $C_4 = \frac{2C_3(\alpha\beta)^{\frac{\alpha+\beta}{2}}}{h_{al}^{C_3}\Gamma(\alpha)\Gamma(\alpha)}$ and $C_5 = \frac{\alpha+\beta-2C_3-2}{2}$.

C. AOA Fluctuations Due to Random Orientation Deviations

The converging lens focuses collected light to the surface on a circular PD. However, due to the random orientation deviations of an aerial node, the angle of arrival of the received beam is deviated from the normal line to the detector area. Indeed, it is crucial to compensate and stabilize the orientation

$$f^{LN}_{h_{ag}|\theta_d}(h_{ag}) = \frac{C_3 {C_1}^{-C_3} h_{ag}^{C_3-1}\cos(\theta_d)}{2h_{al}^{C_3}\sqrt{2\pi\sigma_{Bu}^2}}\sqrt{8\pi\sigma_{Bu}^2}\exp\left(8\sigma_{Bu}^2\left(\left(\frac{2C_3+1}{4}\right)^2-\frac{1}{16}\right)\right). \tag{22}$$

$$f^{GG}_{h_{ag}|\theta_d}(h_{ag}) = \frac{2^{2C_5+1}C_1^{-C_3}h_{ag}^{C_3-1}C_4\cos(\theta_d)}{(4\alpha\beta)^{C_5+1}}\Gamma\left(\frac{2C_5+2+\alpha-\beta}{2}\right)\Gamma\left(\frac{2C_5+2+\beta-\alpha}{2}\right). \tag{23}$$

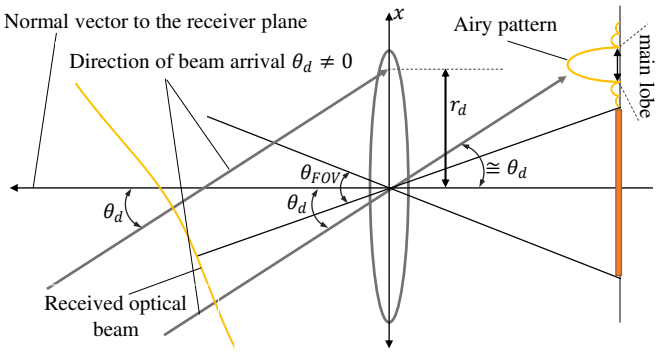

Fig. 4. Configurations of received beam and its diffraction pattern in the presence of AOA fluctuations.

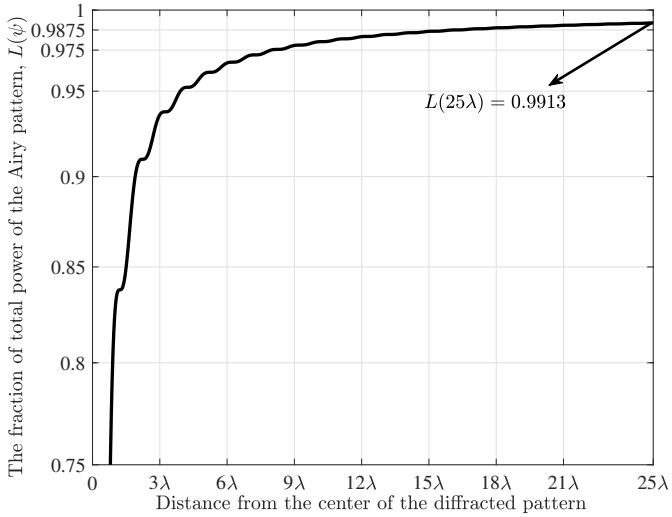

Fig. 5. The fraction of the power of Airy pattern at the PD contained in a circle with radius ψ.

fluctuations of hovering aerial nodes for establishing reliable ground-to-aerial FSO links. More recently, via fast and high accurate stabilization and control systems, the degree of angular instability of the hovering aerial platforms has been shown on the order of several mrad, [50]–[52]. Due to this pinpoint accuracy, it is reasonable to assume that the instantaneous misalignment orientations of the aerial platform, i.e., θ_{Rx} and θ_{Ry}, are sufficiently small and these assumptions enable us to employ small-angle approximation as $\tan(\theta_{Rx}) \simeq \theta_{Rx}$ and $\tan(\theta_{Ry}) \simeq \theta_{Ry}$ [27]. Hence, the RV $\theta_d = \sqrt{\theta_{Rx}^2+\theta_{Ry}^2}$ is approximately Rayleigh distributed with PDF [27]

$$f_{\theta_d}(\theta_d) = \frac{\theta_d}{\sigma_o^2}\exp\left(-\frac{\theta_d^2}{2\sigma_o^2}\right), \qquad \theta_d \geq 0. \tag{24}$$

When an optical beam having small angle of deviation θ_d from the normal vector of aperture plane is passed through a lens, the outside angle of beam will be approximately unchanged [36]. Therefore, as depicted in Fig. 4, AOA fluctuations cause shifted diffracted patterns which can attenuate the amount of received optical power at the PD.

For a circular shape aperture, Airy pattern at the PD consists of a bright disc at the center of the pattern (main-lobe) surrounded by concentric bright and dark rings (side-lobes) [53]. Let h_{af} denote the fraction of power collected by the detector to the power incident in the aperture [27]. Therefore, to calculate the amount of h_{af}, it is essential to explore what fraction of total incident power is contained within the main-lobe and side lobes of the Airy pattern. Let $L(\psi)$ be the fraction of total power of the Airy pattern contained in a circle with radius ψ to the power incident in the aperture. From [53, 8.5 (18)], $L(\psi)$ is obtained as

$$L(\psi) = 1 - J_0^2\left(\frac{\pi\psi}{\lambda}\right) - J_1^2\left(\frac{\pi\psi}{\lambda}\right) \tag{25}$$

where $J_n(\cdot)$ denotes Bessel function of the first kind with order n. To obtain detailed insight into the distribution of the power of Airy pattern at the PD, we plot $L(\psi)$ versus ψ in Fig. 5. As we can observe from this figure, more than 99 percent of the power of the Airy pattern is contained within a circle with radius 25λ, and it is much smaller than the conventional sizes of a PD, which is typically on order of mm [36]. Therefore, when the received laser beam lies inside the receiver FoV, i.e., when $\theta_d \leq \theta_{FOV}$, the total power of the incident beam is captured by the PD. Meanwhile, as thoroughly discussed in [27], ignoring the effect of side-lobes may lead to an incorrect outage probability floor when the receiver FOV is not large enough and the AOA lies outside of the FOV. Accordingly, an accurate approximate expression was proposed for the fading introduced by AOA fluctuations h_{af} for a receiver with a circular PD with radius r_p as [27]

$$h_{af} = \begin{cases} L(r_p) & \theta_d \leq \theta_{\mathrm{FOV}}, \\ \frac{r_p}{4r_d}\Big(L(r_d+r_p) - L(r_d-r_p)\Big) & \text{otherwise.} \end{cases} \tag{26}$$

$$f_h^{LN}(h) \simeq \underbrace{\frac{C_3 {C_1}^{-C_3} h^{C_3-1}}{2h_{al}^{C_3}\sqrt{2\pi\sigma_{Bu}^2}}\sqrt{8\pi\sigma_{Bu}^2}\exp\left(8\sigma_{Bu}^2\left(\left(\frac{2C_3+1}{4}\right)^2-\frac{1}{16}\right)\right)\left(1-e^{-\frac{\theta_{FOV}^2}{2\sigma_\delta^2}}\right)}_{f_h'(h)} + \underbrace{e^{-\frac{\theta_{FOV}^2}{2\sigma_\delta^2}}\delta(h)}_{f_h^0(h)}. \tag{31}$$

From (26) and (28), the PDF of the considered ground-to-HAP link is obtained as

$$f_h(h) = \int_0^\infty h_{af} f_{h_{ag}|\theta_d}(h) f_{\theta_d}(\theta_d) d\theta_d. \tag{27}$$

Nevertheless, the system model of [27] concerns terrestrial FSO links with a narrow receiver FOV, i.e., $0.1 \sim 0.2$ mrad. However, as we will show in the numerical result section, due to the large effect of hovering fluctuations of the HAPs, the optimal FOV for such receivers is on the order of several tens of milli-radians. To make the analysis tractable, we make an approximation to the values of h_{af} by ignoring the effect of sidelobes as follows

$$\tilde{h}_{af} \simeq \Pi\left(\frac{\theta_d}{\theta_{FOV}}\right) \tag{28}$$

where the gate function $\Pi(\cdot)$ is defined as

$$\Pi(x) = \begin{cases} 1 & \text{if } x < 1 \\ 0 & \text{if } x > 1. \end{cases} \tag{29}$$

As it will be shown in the numerical results, the effect of sidelobes is small in such cases as no error floors are observed within the the range of interest of the system performance. Therefore, eq. (28) is a reasonable approximation for systems with large FOV which is the case for HAPs. Thus, eq. (27) can be rewritten as

$$f_h(h) = \int_0^{\theta_{FOV}} f_{h_{ag}|\theta_d}(h) f_{\theta_d}(\theta_d) d\theta_d + \delta(h) \int_{\theta_{FOV}}^\infty f_{\theta_d}(\theta_d) d\theta_d. \tag{30}$$

Nevertheless, it can be cumbersome to evaluate the integral equation in (30). To have a more tractable analytical channel model, for small values of θ_d, we can use small angle approximation as $\cos(\theta_d) \simeq 1$. Accordingly, for small values of h, eq. (30) can be simplified as (31) under LN atmospheric turbulence, and as (32) under GG atmospheric turbulence. Furthermore, based on (31) and (32), closed-form expressions for the outage probabilities are derived in (33) and (34), respectively, for LN and GG atmospheric turbulence models.

IV. Simulation Results and Analysis

In this section, we illustrate the analytical results derived in the previous sections. We evaluate the link performance in terms of the outage probability and study the impact of different parameters, i.e., the FoV of the receiver and its orientation deviations, and the beam spot size at the transmitter, on the performance of the ground-to-HAP link. Meanwhile, the accuracy of the derived analytical expressions is corroborated by Monte Carlo simulations using over 4×10^6 independent runs. Simulations are performed based on the practical values of the parameters outlined in Table I [54]. Since the height of the receiver, H, is much larger than the height of the optical transmitter, h_0, without loss of generality, we neglect the height of the transmitter for calculating the link length Z (i.e., we assume that h_0 is equal to zero). We consider a strong turbulence model for atmospheric turbulence, i.e., GG model, however, the results and discussions can be readily developed to weak turbulence scenarios by applying the LN model and its related expressions in Section III.

TABLE I
Nominal Values Used for the Numerical Results

Name	Parameter	Value
Optical wavelength	λ	1550 nm
PD responsibility	η	0.9
Optical bandwidth of the receiver	B_o	10 nm
Receiver electrical bandwidth	B_e	1 GHz
Spectral radiance of the background radiation at λ	$N_b(\lambda)$	10^{-3} W/cm^2-m-srad
HAP zenith angle	ζ	40°
Link length	Z	20 km
The RMS of wind speed	V_ω	21 m/s
Electron charge	e	1.6×10^{-19}
Refractive index structure at the ground	$C_n^2(0)$	1.7×10^{-13} m$^{-2/3}$

First, we show in Figs. 6 and 7, respectively, the channel distribution under both LN and GG atmospheric turbulence for different values of w_Z/r_a. From these two figures we observe that the accuracy of the derived analytical channel model depends on the ratio of w_Z and r_a. Since aperture radius in FSO systems is on the order of several centimeters and also, for long-range ground-to-HAP links, w_Z is on the order of several meters, the proposed analytical expression for the channel model of such links achieves acceptable level of accuracy. Therefore, the system performance metrics for a ground-to-HAP FSO link, e.g., outage probability, and bit error rate can be analytically developed without resorting to time-consuming simulations.

To broaden our understanding about the impact of orientation deviations due to hovering fluctuations of the receiver on the link performance, we plot outage probability versus

$$f_h^{GG}(h) \simeq \underbrace{\frac{2^{2C_5+1}C_1^{-C_3}h^{C_3-1}C_4}{(4\alpha\beta)^{C_5+1}}\Gamma\left(\frac{2C_5+2+\alpha-\beta}{2}\right)\Gamma\left(\frac{2C_5+2+\beta-\alpha}{2}\right)\left(1-e^{-\frac{\theta_{FOV}^2}{2\sigma_o^2}}\right)}_{f_h'(h)} + \underbrace{e^{-\frac{\theta_{FOV}^2}{2\sigma_o^2}}\delta(h)}_{f_h^0(h)}. \tag{32}$$

$$\mathbb{P}_{\text{out}}^{LN} = e^{-\frac{\theta_{FOV}^2}{2\sigma_o^2}} + \frac{C_3C_1^{-C_3}h_{\text{th}}^{C_3}}{2C_3h_{al}^{C_3}\sqrt{2\pi\sigma_{Bu}^2}}\sqrt{8\pi\sigma_{Bu}^2}\exp\left(8\sigma_{Bu}^2\left(\left(\frac{2C_3+1}{4}\right)^2-\frac{1}{16}\right)\right)\left(1-e^{-\frac{\theta_{FOV}^2}{2\sigma_o^2}}\right). \tag{33}$$

$$\mathbb{P}_{\text{out}}^{GG} = e^{-\frac{\theta_{FOV}^2}{2\sigma_o^2}} + \frac{2^{2C_5+1}C_1^{-C_3}h_{\text{th}}^{C_3}C_4}{(4\alpha\beta)^{C_5+1}C_3}\Gamma\left(\frac{2C_5+2+\alpha-\beta}{2}\right)\Gamma\left(\frac{2C_5+2+\beta-\alpha}{2}\right)\left(1-e^{-\frac{\theta_{FOV}^2}{2\sigma_o^2}}\right). \tag{34}$$

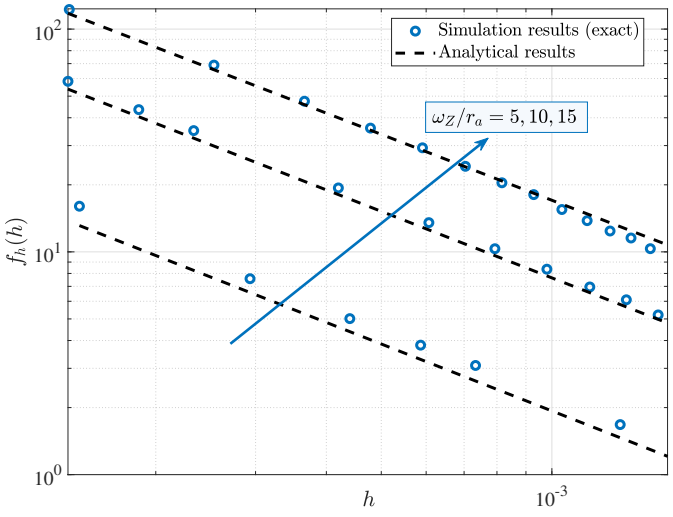

Fig. 6. Channel distribution $f_h(h>0)$, for different values of w_Z/r_a, under Log-normal atmospheric turbulence.

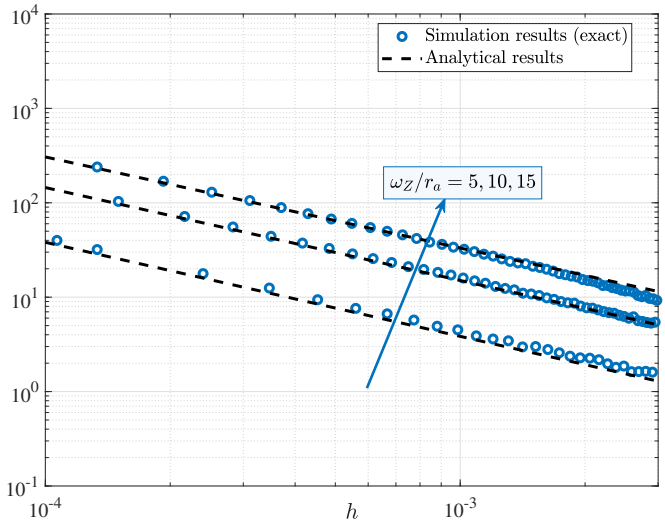

Fig. 7. Channel distribution $f_h(h>0)$, for different values of w_Z/r_a, under Gamma-Gamma atmospheric turbulence.

P_t for different values of σ_0^2 in Fig. 8. As shown, an exact match between the analytical and simulation-based results can be observed, which validates the accuracy of the derived analytical expression for the outage probability. Also, as we can observe from this figure, the performance of such links largely depends on the AOA fluctuations due to random orientation deviations of the HAP, and, as expected, the outage probability increases when AOA fluctuations at the receiver side is increased. However, such performance degradation can be improved by increasing the receiver FOV. On the other hand, an increase of FOV of the receiver also increases the amount of undesired background noise, which adversely affects the link performance. To study the inherent tradeoff in optimizing the receiver FOV, we plot outage probability versus P_t for different values of the receiver FOV and for $\sigma_0^2 = 15$ mrad in Fig. 9. As shown, from Fig. 9, for given values of AOA fluctuations, the link performance is sensitive to the amount of the receiver FOV. Moreover, from Fig. 10, one can realize that increasing the amount of FOV does not necessarily improve the system performance. Figs. 9 and 10 demonstrate the importance of designing optimal receiver FOV to alleviate the impacts of AOA fluctuations on the performance of the ground-to-HAP FSO links. The optimal θ_{FOV} values to achieve minimum outage probability over the considered ground-to-HAP FSO link for different values of σ_0 are provided in Table II. The analytical results of this table

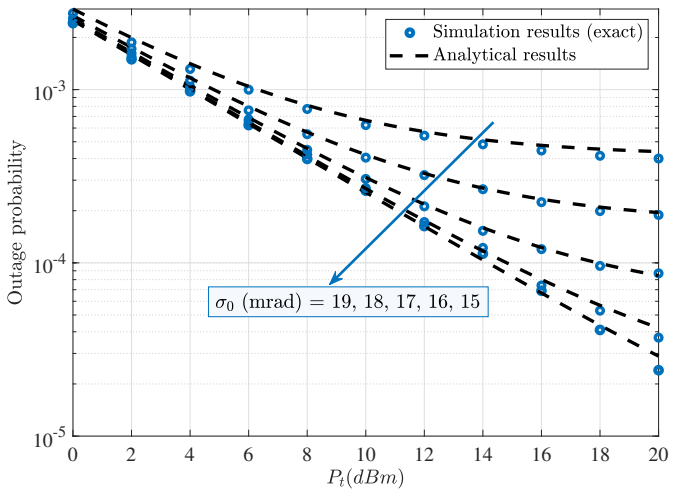

Fig. 8. Outage probability versus P_t for $w_Z/r_a = 20$, $\theta_{\text{FOV}} = 75$ mrad, $\sigma_d = 0.4$ m, and different values of the orientation deviations σ_0.

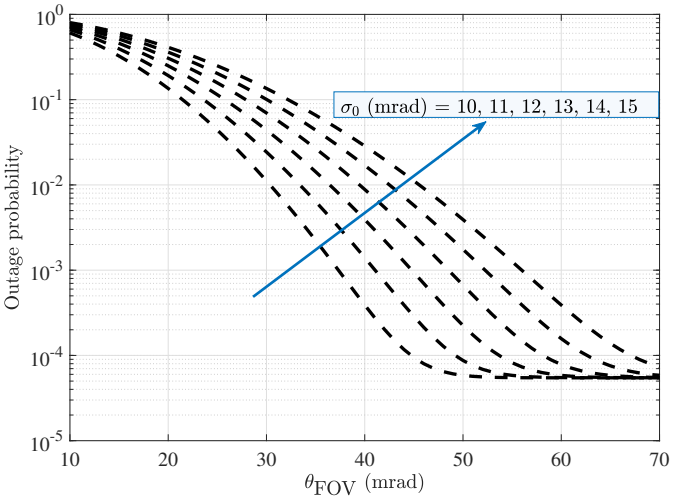

Fig. 10. Outage probability versus θ_{FOV} for $W_Z/r_a = 20$, $\sigma_d = 0.4$ m, and different values of the orientation deviations σ_0.

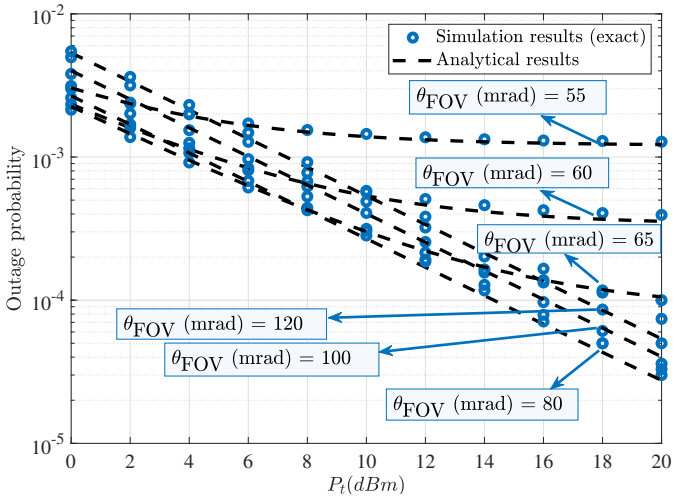

Fig. 9. Outage probability versus P_t for $w_Z/r_a = 20$, $\sigma_0 = 15$ mrad, $\sigma_d = 0.4$ m, and different values of the receiver FOV θ_{FOV}.

Table II
OPTIMAL VALUES OF θ_{FOV} TO ACHIEVE MINIMUM OUTAGE PROBABILITY OVER GROUND-TO-HAP LINK FOR DIFFERENT VALUES OF σ_0.

	$P_t = 5$ dBm, $w_Z/r_a = 10$, and σ_d = 0.2 m		
σ_0 (mrad)	θ_{FOV} (mrad)	Outage probability	
		Simulation results	Analytical results
5	26	8.0×10^{-6}	2.3×10^{-7}
8	70	2.60×10^{-5}	3.76×10^{-5}
10	96	3.2×10^{-5}	2.00×10^{-5}
12	104	4.5×10^{-5}	6.01×10^{-5}
14	122	4.6×10^{-5}	6.51×10^{-5}
16	139	5×10^{-5}	7.5×10^{-5}
18	156	8.2×10^{-5}	8.00×10^{-5}

are obtained by differentiating (34) with respect to θ_{FOV} and setting the result equal to zero. Meanwhile, Table II confirms the accuracy of the proposed analytical expressions for outage probability, making it easy to study and design such HAP-based FSO communication links under the degree of instability of the HAP (i.e., the amount of hovering fluctuations).

Figure 11 investigates the performance of the considered link by presenting outage probability as the values of transmit power P_t and the beam-width of the transmitter w_Z vary. From this figure, for a given variance of pointing error, it is clear that the outage performance largely depends on the values of w_Z, and increasing w_Z does not necessarily decrease the amount of the outage probability. Indeed, the effect of w_Z on the outage probability is significant at low transmit power P_t. Fig. 11 highlights the need to optimize w_Z for improving system performance by alleviating the impacts of increasing irradiance fluctuations and beam wander on the performance of the considered link. Accordingly, the optimal w_Z values and the corresponding outage probabilities obtained from both analytical and simulation results are shown in Table III for different values of orientation deviations. These results can be applied to find the optimal values of w_Z for different amount of orientation deviations. Our analytical approach facilitates the design of ground-to-HAP FSO links without resorting to time-consuming simulations. Moreover, in order to have more intuition for link designing and carrying out some tests on the considered link, we have provided the outage probability curves versus SNR for different values of the transmit divergence angle, θ_{div}, in Fig. 12. Again, the results of this figure clearly show that choosing the optimal values of θ_{div} can considerably help to mitigate the effect of AOA fluctuations on the link performance. For instance, when the transmit beam-width is not wide enough, i.e., θ_{div} 0.1 or 0.2 mrad, an outage probability floor can be noticed due to the dominant effect of AOA fluctuations on the link.

Finally, by using the optimal values of w_Z and θ_{FOV} obtained from Tables II and III, we study in Fig. 13 the effect of increasing irradiance fluctuations and beam wander caused by increasing ζ (or equally increasing the link length Z) on link budget. From Fig. 13 and under a given degree of instability of the HAP, we can conclude that the same system performance for different link lengths can be delivered by employing optimal values for w_Z and θ_{FOV} and also bearing

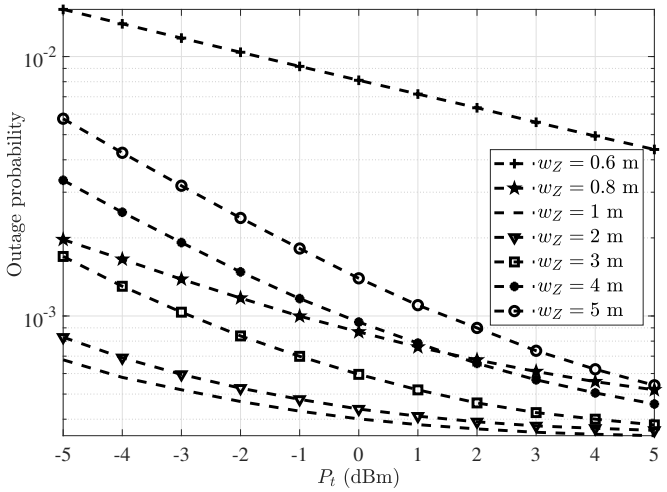

Fig. 11. Outage probability versus P_t for $r_a = 5$ cm, $\sigma_d = 0.4$ m, $\sigma_0 = 5$ mrad and different values of w_Z.

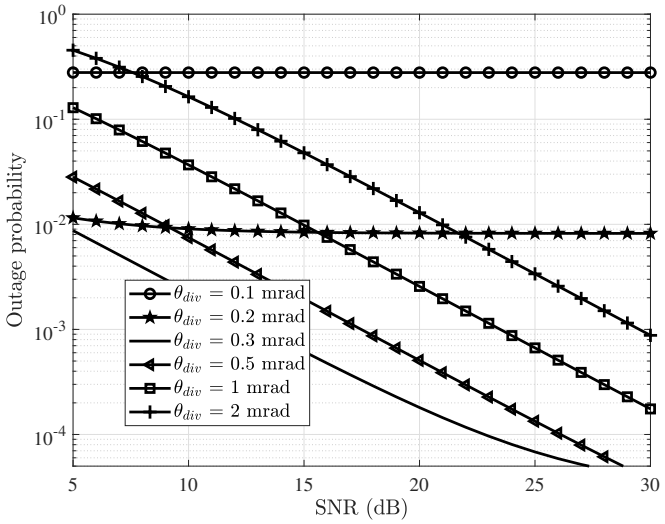

Fig. 12. Outage probability versus SNR for $r_a = 10$ cm, $\sigma_d = 1$ m, $\sigma_0 = 15$ mrad, $Z = 15$ km, and different values of θ_{div}.

the cost of increasing the link budget. For instance, to have a same value in outage probability, the change in ζ from 10° to 60° will increase transmit power by 2 dBm.

V. CONCLUSION

We studied the problem of integrating FSO communication into HAPs for providing high data rate wireless connectivity. To facilitate design of a ground-to-HAP FSO link, we proposed simple and tractable statistical models for channel model under both LN and GG atmospheric turbulence considerations. The proposed models incorporate the combined effects of position vibrations of the receiver, pointing jitter variance caused by beam wander, detector aperture size, received optical beam-width, the FOV of the receiver, atmospheric attenuation and turbulence, and the AOA fluctuations of the received optical beam. Subsequently, closed-form expressions

Table III
OPTIMAL VALUES OF W_z TO ACHIEVE MINIMUM OUTAGE PROBABILITY OVER GROUND-TO-HAP LINK FOR DIFFERENT VALUES OF σ_d.

	$P_t = 5$ dBm, $\theta_{FOV} = 45$ mrad, and $\sigma_0 = 10$ mrad		
σ_d (m)	w_Z (m)	Outage probability	
		Simulation results	Analytical results
0.1	0.25	3.90×10^{-5}	1.13×10^{-5}
0.2	0.49	4.8×10^{-5}	2.84×10^{-5}
0.3	0.74	4.9×10^{-5}	4.04×10^{-5}
0.4	1.10	5.3×10^{-5}	4.06×10^{-5}
0.6	1.35	1.86×10^{-4}	1.03×10^{-4}
0.8	2.20	2.42×10^{-4}	1.2×10^{-4}
1	2.8	4.41×10^{-4}	3.10×10^{-4}

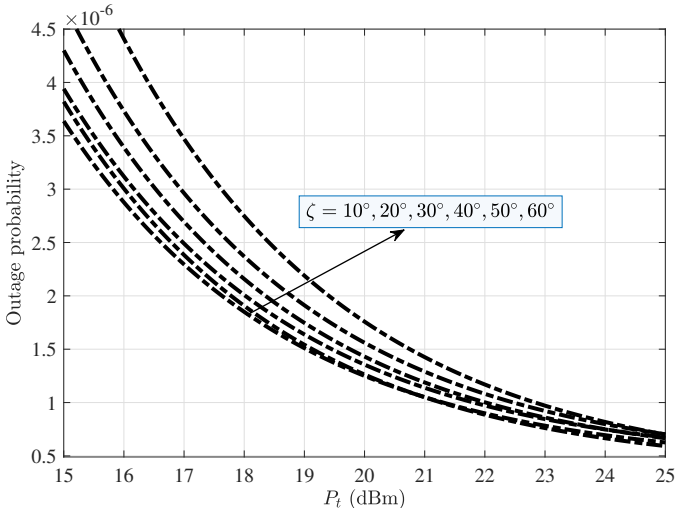

Fig. 13. Outage probability versus P_t for $\sigma_0^2 = 10$ mrad, $H = 17$ km, and different values of the zenith angle ζ (for each ζ, w_Z is chosen optimally to achieve minimum outage probability).

are derived for the outage probability of the considered link under different turbulence regimes. The developed models make it possible to conduct detailed analysis towards optimizing the transmitted laser beam and the FOV of the receiver in terms of achieving minimum outage probability under different channel conditions. We showed that the performance of such links largely depends on the receiver FOV and the received optical beam-width ω_Z. Thus, the results of this paper can be used for finding the optimal values of link parameters and designing ground-to-HAP FSO links without resorting to time-consuming simulations.

REFERENCES

[1] M. Mozaffari, W. Saad, M. Bennis, Y. H. Nam, and M. Debbah, "A tutorial on UAVs for wireless networks: Applications, challenges, and open problems," *IEEE Commun. Surveys Tuts.*, Mar. 2019.

[2] S. Karapantazis and F. Pavlidou, "Broadband communications via high-altitude platforms: A survey," *IEEE Commun. Surveys Tuts.*, vol. 7, no. 1, pp. 2–31, May 2005.

[3] M. Mozaffari, W. Saad, M. Bennis, and M. Debbah, "Mobile unmanned aerial vehicles (UAVs) for energy-efficient internet of things communications," *IEEE Trans. Wireless Commun.*, vol. 16, no. 11, pp. 7574–7589, Nov. 2017.

[4] M. Alzenad, M. Z. Shakir, H. Yanikomeroglu, and M. S. Alouini, "FSO-based vertical backhaul/fronthaul framework for 5G+ wireless networks," *IEEE Commun. Mag.*, vol. 56, no. 1, pp. 218–224, Jan. 2018.

[5] Y. Dong, M. Z. Hassan, J. Cheng, M. J. Hossain, and V. C. Leung, "An edge computing empowered radio access network with UAV-mounted FSO fronthaul and backhaul: Key challenges and approaches," *IEEE Wireless Commun.*, vol. 25, no. 3, pp. 154–160, June 2018.

[6] Google,"Project Loon," [online] https://x.company/loon/.

[7] Facebook,"Internet.org by Facebook," [online] https://internet.org/.

[8] C. M. Schieler *et al.*, "NASA's Terabyte Infrared Delivery (TBIRD) Program: Large-Volume Data Transfer from LEO," *33rd Annual AIAA/USU Conference on Small Satellites*, pp. SSC19–VI–02, 2020.

[9] E. Y. Luzhansky *et al.*, "Laser communications relay demonstration." *SPIE*, vol. 9739, pp. 102 – 113, Mar. 2016.

[10] H. Safi, A. Dargahi, and J. Cheng, "Spatial beam tracking and data detection for an FSO link to a UAV in the presence of hovering fluctuations," *arXiv preprint arXiv:1904.03774*, 2019.

[11] M. Khan, M. Yuksel, and G. Winkelmaier, "GPS-free maintenance of a free-space-optical link between two autonomous mobiles," *IEEE Trans. Mobile Comput.*, vol. 16, no. 6, pp. 1644–1657, June 2017.

[12] A. Kaadan, H. Refai, and P. Lopresti, "Spherical FSO receivers for UAV communication: Geometric coverage models," *IEEE Trans. Aerosp. Electron. Syst.*, vol. 52, no. 5, pp. 2157–2167, Oct. 2016.

[13] Y. Kaymak, R. Rojas-Cessa, J. Feng, N. Ansari, M. Zhou, and T. Zhang, "A survey on acquisition, tracking, and pointing mechanisms for mobile free-space optical communications," *IEEE Commun. Surveys Tuts.*, vol. 20, no. 2, pp. 1104–1123, Feb. 2018.

[14] L. C. Andrews and R. L. Phillips, *Laser Beam Propagation through Random Media*. SPIE Press Bellingham, WA, 2005.

[15] T. Song and P.-Y. Kam, "A robust GLRT receiver with implicit channel estimation and automatic threshold adjustment for the free space optical channel with IM/DD," *J. Lightw. Technol.*, vol. 32, no. 3, pp. 369–383, Feb. 2014.

[16] M. T. Dabiri, S. M. S. Sadough, and H. Safi, "GLRT-based sequence detection of OOK modulation over FSO turbulence channels," *IEEE Photon. Technol. Lett.*, vol. 29, no. 17, pp. 1494–1497, Jan. 2017.

[17] A. Jaiswal, M. Abaza, M. R. Bhatnagar, and V. K. Jain, "An investigation of performance and diversity property of optical space shift keying based FSO-MIMO system," *IEEE Trans. Commun.*, vol. 66, no. 9, pp. 4028–4042, Mar. 2018.

[18] J. A. Mendenhall *et al.*, "Design of an optical photon counting array receiver system for deep-space communications," *in Proceedings of the IEEE*, vol. 95, no. 10, pp. 2059–2069, Oct. 2007.

[19] I. I. Kim, H. Hakakha, P. Adhikari, E. J. Korevaar, and A. K. Majumdar, "Scintillation reduction using multiple transmitters." *SPIE*, vol. 2990, pp. 102 – 113, Apr. 1997.

[20] H. Safi, A. A. Sharifi, M. T. Dabiri, I. S. Ansari, and J. Cheng, "Adaptive channel coding and power control for practical FSO communication systems under channel estimation error," *IEEE Trans. Vehic. Technol.*, vol. 68, no. 8, pp. 7566–7577, Aug. 2019.

[21] R. K. Tyson, "Bit error rate for free space adaptive optics laser communications," *J. Opt. Soc. Amer. A, Opt. Image Sci.*, vol. 19, no. 4, pp. 753–758, Apr. 2002.

[22] A. K. Majumdar and J. C. Riclkin, *Free-Space Laser Communications: Principles And Advances*. Springer-Verlag, New York, NY, USA, 2007.

[23] H. Hemmati, *Deep Space Optical Communications*. Wiley-Interscience, Hoboken, NJ, USA, 2006.

[24] M. A. Khalighi and M. Uysal, "Survey on free space optical communication: A communication theory perspective," *IEEE Commun. Surveys Tuts.*, vol. 16, no. 4, pp. 2231–2258, Nov. 2014.

[25] H. Kaushal and G. Kaddoum, "Optical communication in space: Challenges and mitigation techniques," *IEEE Commun. Surveys Tuts.*, vol. 19, no. 1, pp. 57–96, Aug. 2017.

[26] B. G. D. D. L. B. Stotts, P. K. A. Pike and J. Douglass, "Free-space optical communications link budget estimation," *Appl. Opt.*, vol. 49, no. 28, pp. 5333–5343, Oct. 2010.

[27] S. Huang and M. Safari, "Free-space optical communication impaired by angular fluctuations," *IEEE Trans. Wireless Commun.*, vol. 16, no. 11, pp. 7475–7487, Nov. 2017.

[28] W. Fawaz, C. Abou-Rjeily, and C. Assi, "UAV-aided cooperation for FSO communication systems," *IEEE Commun. Mag.*, vol. 56, no. 1, pp. 70–75, Jan. 2018.

[29] L. Yang, J. Yuan, X. Liu, and M. O. Hasna, "On the performance of LAP-Based Multiple-Hop RF/FSO systems," *IEEE Trans. Aerosp. Electron. Syst*, vol. 55, no. 1, pp. 499–505, Feb. 2019.

[30] L. Li, R. Zhang, Z. Zhao, G. Xie, P. Liao, K. Pang, H. Song, C. Liu, Y. Ren, G. Labroille *et al.*, "80-Gbit/s 100-m free-space optical data transmission link via a flying UAV using multiplexing of orbital-angular-momentum beams," *arXiv preprint arXiv:1708.02923*, 2017.

[31] V. Mai and H. Kim, "Beam size optimization and adaptation for high-altitude airborne free-space optical communication systems," *IEEE Photon. J.*, vol. 11, no. 2, pp. 1–13, Feb. 2019.

[32] M. Li, Y. Hong, C. Zeng, Y. Song, and X. Zhang, "Investigation on the UAV-to-satellite optical communication systems," *IEEE J. Sel. Areas Commun.*, vol. 36, no. 9, pp. 2128–2138, Sep. 2018.

[33] M. T. Dabiri, S. M. S. Sadough, and M. A. Khalighi, "Channel modeling and parameter optimization for hovering UAV-based free-space optical links," *IEEE J. Sel. Areas Commun.*, vol. 36, no. 9, pp. 2104–2113, Sep. 2018.

[34] M. T. Dabiri, S. M. S. Sadough, and I. S. Ansari, "Tractable optical channel modeling between UAVs," *IEEE Trans. Vehic. Technol.*, Sep. 2019 (early access).

[35] M. Najafi, H. Ajam, V. Jamali, P. D. Diamantoulakis, G. K. Karagiannidis, and R. Schober, "Statistical modeling of the fso fronthaul channel for uav-based networks," *arXiv preprint arXiv:1905.12424*, 2019.

[36] R. M. Gagliardi and S. Karp, *Optical Communications*. New York, Wiley-Interscience, 1995.

[37] X. Zhu and J. M. Kahn, "Free-space optical communication through atmospheric turbulence channels," *IEEE Trans. Commun.*, vol. 50, no. 8, pp. 1293–1300, Aug. 2002.

[38] M. T. Dabiri, S. M. S. Sadough, and M. A. Khalighi, "FSO channel estimation for OOK modulation with APD receiver over atmospheric turbulence and pointing errors," *Opt. Commun.*, vol. 402, pp. 577–584, Nov. 2017.

[39] A. Carrasco-Casado, J. M. Sánchez-Pena, and R. Vergaz, "CTA telescopes as deep-space lasercom ground receivers," *IEEE Photon. Journal.*, vol. 12, no. 4, pp. 1–4, Nov. 2015.

[40] S. Riechelmann, M. Schrempf, and G. Seckmeyer, "Simultaneous measurement of spectral sky radiance by a non-scanning multidirectional spectroradiometer (MUDIS)," *Measurement Science and Technology*, vol. 24, no. 12, p. 125501, Nov. 2013.

[41] E. E. Bell, L. Eisner, J. Young, and R. A. Oetjen, "Spectral radiance of sky and terrain at wavelengths between 1 and 20 microns. ii. sky measurements," *JOSA*, vol. 50, no. 12, pp. 1313–1320, Dec. 1960.

[42] H. Hemmati, *Deep Space Optical Communications*. Wiley-Interscience,, Hoboken, NJ, USA, 2006.

[43] A. A. Farid and S. Hranilovic, "Outage capacity optimization for free-space optical links with pointing errors," *IEEE/OSA J. Light. Technol.*, vol. 25, no. 7, pp. 1702–1710, July 2007.

[44] M. C. Al Naboulsi, H. Sizun, and F. de Fornel, "Fog attenuation prediction for optical and infrared waves," *Opt. Eng.*, vol. 43, no. 2, pp. 319–330, Feb. 2004.

[45] R. E. Hufnagel, *Variations of Atmospheric Turbulence*. Tech. Report, 1974.

[46] R. K. Tyson, "Adaptive optics and ground-to-space laser communication," *Appl. Opt.*, vol. 35, no. 19, pp. 3640–3646, July 1996.

[47] G. C. Valley, "Isoplanatic degradation of tilt correction and short-term imaging systems," *Appl. Opt.*, vol. 19, no. 4, pp. 574–577, Feb. 1980.

[48] B. E. Saleh and M. C. Teich, *Fundamentals of Photonics*. John Wiley & Sons, 2019.

[49] A. E. Siegman, *Lasers University Science Books*. Mill Valley, CA, 1986.

[50] M. Orsag, C. Korpela, S. Bogdan, and P. Oh, "Dexterous aerial robots—mobile manipulation using unmanned aerial systems," *IEEE Trans. Robot.*, vol. 33, no. 6, pp. 1453–1466, Dec. 2017.

[51] H. Lee and H. J. Kim, "Estimation, control, and planning for autonomous aerial transportation," *IEEE Trans. Indus. Elec.*, vol. 64, no. 4, pp. 3369–3379, Aug. 2017.

[52] M. Faessler, D. Falanga, and D. Scaramuzza, "Thrust mixing, saturation, and body-rate control for accurate aggressive quadrotor flight," *IEEE Robot. Automat. Lett.*, vol. 2, no. 2, pp. 476–482, Dec. 2017.

[53] M. Born and E. Wolf, *Principles of Optics: Electromagnetic Theory of Propagation, Interference and Diffraction of Light*. Cambridge Univ. Press, 1999.

[54] Z. Ghassemlooy, W. Popoola, and S. Rajbhandari, *Optical Wireless Communications*. CRC Press Boca Raton, FL, 2012.